Journal of Orthopaedic Translation 33 (2022) 1–12

Contents lists available at ScienceDirect

Journal of Orthopaedic Translation

journal homepage: www.journals.elsevier.com/journal-of-orthopaedic-translation

A mouse model of disuse osteoporosis based on a movable noninvasive 3D-printed unloading device

Junhui Li [a], Jiangyu Geng [a], Tingting Lin [a], Mingxiang Cai [b], Yao Sun [a,*]

[a] Department of Oral Implantology, School of Stomatology, Tongji University, Shanghai Engineering Research Center of Tooth Restoration and Regeneration, Shanghai, China

[b] The First Affiliated Hospital of Jinan University, School of Stomatology, Clinical Research Platform for Interdisciplinary Stomatology, Jinan University, Guangzhou, China

ARTICLE INFO

Keywords:
Disuse osteoporosis
Unloaded osteoporosis mouse model
Bone loss
Noninvasive
3D printing

ABSTRACT

Objective: Disuse osteoporosis is a major type of bone loss disease characterized by regional bone loss and microstructure alterations. The condition is induced by a marked decrease in weight bearing over time, which usually occurs due to limb immobilization, therapeutic bed rest or space flight. To date, the most commonly used mouse model of disuse osteoporosis is constructed using the classical tail suspension method, which causes tail injury, movement inconvenience and mental stress. This study aimed to propose a noninvasive and effective method for the establishment of a mouse model of disuse osteoporosis and compared this method with the tail suspension method.

Methods: 3D printing technology was applied to construct a movable unloading device. A movable noninvasive 3D-printed unloading device (3D-ULD) was used to unload the hindlimbs of the mice. The bone microstructure and bone volume of unloaded femurs were analysed through micro-CT and H&E staining, and *von Kossa* staining was performed for the detection of bone mineralization in the femurs. TRAP staining, IHC-CTSK and Q-PCR were performed for evaluation of the bone resorption ability, and double labelling, IHC-DMP1, ALP staining and Q-PCR assays were conducted to assess the osteogenic ability. The mechanical properties of disused bone were detected using the three-point bending test. The body, thymus and spleen weights of the mice were recorded, and the serum corticosterone level of the mice was assayed by enzyme-linked immunosorbent assay (ELISA).

Results: The micro-CT results showed significant trabecular bone loss, and 3D-ULD induced cortical bone loss in disused femurs as well as a decrease in the bone mineral density in the unloaded mice. TRAP staining and IHC-CTSK staining results indicated increases in the osteoclast number per bone perimeter (Oc.N/B.Pm) and the osteoclast surface per bone surface (Oc.S/BS) in the unloaded mice. The *Ctsk*, *Trap* and *Mmp9* expression levels were significantly increased in the unloaded mice. Decreases in the ratio of the mineral surface to bone surface (MS/BS), mineral apposition rate (MAR) and bone formation rate per bone surface (BFR/BS) were found in unloaded mice in the 3D-ULD by double labelling. The IHC-DMP1 and ALP staining results showed decreases in the osteoblast number per bone perimeter (Ob.N/B.Pm) and osteoblast surface per bone surface (Ob. S/BS) in the mice unloaded in the 3D-ULD, and these mice also showed decreased *Runx2*, *Alp* and *Dmp1* expression levels. Three-point bending test results showed that the mechanical properties were attenuated in the disused femurs of the unloaded mice. Less skin rupture and rare alterations in the thymus and spleen weights were found in the unloaded mice in the 3D-ULD. The ELISA results indicated the serum corticosterone level of the mice unloaded in the 3D-ULD was significantly lower than that of mice suspended by their tail.

Conclusion: This new disuse osteoporosis mouse model based on 3D-ULD could induce effective disuse bone loss with significantly alleviated side effects.

Translational potential of this article: This study proposes a new disuse osteoporosis mouse model based on 3D-ULD that can be used to better understand disuse bone loss in the future.

* Corresponding author. School of Stomatology, Tongji University, Shanghai, 200072, China.
E-mail address: yaosun@tongji.edu.cn (Y. Sun).

https://doi.org/10.1016/j.jot.2021.11.009
Received 26 August 2021; Received in revised form 2 November 2021; Accepted 22 November 2021

1. Introduction

Osteoporosis, which is a common metabolic disease with a high incidence in elderly individuals, manifests as a seriously low bone mass, pathological alterations in the bone microstructure and a greatly increased risk of fracture [1]. Traditionally, osteoporosis is divided into primary and secondary osteoporosis. Primary osteoporosis is normally independent of other chronic diseases and refers to osteoporosis involving senility or gonadal function decline, such as postmenopausal osteoporosis [2]. Conversely, secondary osteoporosis usually results from other health issues, among which disuse is one of the main causes [3]. Reductions in weight bearing over time causes regional bone loss and microstructure alterations at weight-bearing bone sites [4]. Due to the elimination of weight-bearing physical activity, disuse osteoporosis usually results from limb immobilization, therapeutic bed rest and space flight and has become a nonnegligible health problem.

Due to the limitations of clinical research, the establishment of a suitable animal model is a key precondition for in-depth investigations of bone damage due to disuse. Several methods have been developed for the construction of animal models of disuse osteoporosis, and these methods include tail suspension and hindlimb immobilization by sciatic neurectomy, tenotomy or use of a plaster cast [5–8]. Although these methods can induce osteoporosis in animals, they have obvious disadvantages. Sciatic neurectomy immobilizes the hindlimbs by destroying the sciatic nerve and thereby causing alterations in key neurotrophic factors that affect bone metabolism [9]. Tenotomy, in which knee tendons are severed to immobilize the limbs, is an invasive method for inducing disuse osteoporosis [10]. Moreover, the abovementioned models are not suitable for reversibility studies. In some cases, bone loss is even slowly induced because the hindlimbs of animals still partially bear weight [11]. The tail suspension method is the most commonly used approach for inducing disuse osteoporosis in mice and rats and was originally designed to simulate the low gravity experienced by astronauts [12,13]. However, suspended animals suffer discomfort, chronic stress and even pain and cannot move or eat freely. Moreover, due to trauma to the tail, animals are rarely suspended for a long time using the tail suspension method [14]. Therefore, to better investigate disuse osteoporosis, the identification of novel methods that can effectively achieve disuse bone loss without harming the animal is urgently needed.

3D printing technology is a rapid prototyping technology that combines intelligent digital manufacturing and material science. The use of 3D printing technology, which is characterized by high precision and good customization capabilities, can effectively satisfy many special requirements in the field of medicine and currently plays significant roles in medical models, artificial organs and tissue regeneration [15,16]. In this study, we created an innovative disuse osteoporosis mouse model based on 3D printing technology to overcome the abovementioned shortcomings. Mice were supported by a movable noninvasive 3D-printed unloading device (3D-ULD), which is a personalized device that can be freely modulated to adjust to the increasing body size of a growing mouse. The mice can move freely by their forelimbs when unloaded in the 3D-ULD. To evaluate the effectiveness of this new method for constructing a mouse model of disuse osteoporosis, histomorphological, molecular biological and mechanical experiments were conducted, and the model was subjected to head-to-head comparisons with the tail suspension-based model. The experimental results showed that this unloading method using 3D-ULD could effectively induce disuse osteoporosis with greater consideration for animal welfare and exerted no obvious traumatic effects on the mice.

2. Materials and methods

2.1. Animal information

Male C57BL/6 J mice were purchased from Shanghai Legen Biotechnology Co., Ltd. The mice were housed in a specific pathogen-free facility under controlled temperature and humidity conditions and subjected to a 12-h light/dark schedule. Disuse osteoporosis was induced in 3-month-old male mice through tail suspension or the use of 3D-ULD for 1 month. The experimental groups consisted of the control group (4-month-old male mice), the tail suspension group (3-month-old male mice suspended by their tail for 1 month) and the 3D-ULD unloaded group (3-month-old male mice unloaded in the 3D-ULD for 1 month). To assess the bone loss of mice unloaded in the 3D-ULD over time, a 2-month unloaded group was also established (2-month-old male mice unloaded in the 3D-ULD for 2 months). One mouse detached from the unloading device and accidently fell during the 1-month unloading period, and two mice detached during the 2-month unloading period. One mouse in the tail suspension group fell from the suspension device. All mice that fell from the device were eliminated from the study, and new mice were added to the group. Each group consisted of six mice. The body weight of the mice was recorded every seven days.

2.2. Study approval

All animals were bred according to the National Institutes of Health's Guide for the Care and Use of Laboratory Animals. This study was approved by the Ethics Committee and the Institutional Animal Care and Use Committee of Tongji University (2019-DW-040). This study conformed to the ARRIVE guidelines.

2.3. Design of the 3D-printed unloading device

Various body parameters of the mice, including the body length, width, thickness of the tail (1/3 proximal part) and positions of the hip joint, were measured. To support the posterior parts of the mouse during unloading of the hindlimbs, a frame with a middle supporting cavity was proposed. For evaluation of the mouse at an appropriate 30-degree forward inclination similar to that observed with the tail suspension method, the height of the bearing surface of the middle supporting cavity was determined based on the length of the mouse body and the positions of the hip joint. Moreover, to fix the tail such that the mouse is maintained at a tilted angle and their hindlimbs are unloaded, a small cavity with a cushion in the upper part of the frame was designed in accordance with the width of the tail. The different body sizes of the individual mice and the increasing body size of each growing mouse were considered; therefore, rotary knobs with cushions, which could be freely modulated to accommodate the individual size of each mouse, were added to the lateral sides of the frame. To ensure free movement of the mouse in the unloading device, wheels were assembled under the frame. The 3D-ULD was designed using Rhino (Version 5.0). A schematic diagram of the 3D-ULD is shown in Fig. 1A. The exact parameters of the 3D-ULD used in this study were as follows. The height and width of the 3D-ULD were 65.5 mm and 91.8 mm, respectively, and the thickness of the 3D-ULD was 10.6 mm. The maximum width and height of the middle cavity were 30.6 mm and 20.1 mm, respectively. The diameter of the upper cavity in the frame was 6.0 mm. The three semilunar cushions were printed using a 3D printing machine (Lite 600, Union Tech, Shanghai, China) with soft rubber material, and the rest of the parts of the unloading device (except for the wheels and wheel axles) were printed with photosensitive resin. The total weight of the 3D-ULD used in this study was 16.9 g.

2.4. Experimental design of disuse osteoporosis using the 3D-ULD

After anaesthesia through the intraperitoneal injection of 80 mg/kg pentobarbital sodium, each mouse was gently placed in the 3D-ULD. The modelling process of disuse osteoporosis is shown in Fig. 1B. In brief, we placed the abdomen of the mouse in the middle of the supporting cavity of the frame to tilt the mouse forward and thereby maintain its hindlimbs out of contact with the ground. The unloaded mice were placed at a head-down angle of approximately 30° based on the tail suspension method as a reference. We then modulated the horizontal rotary knobs to fit the

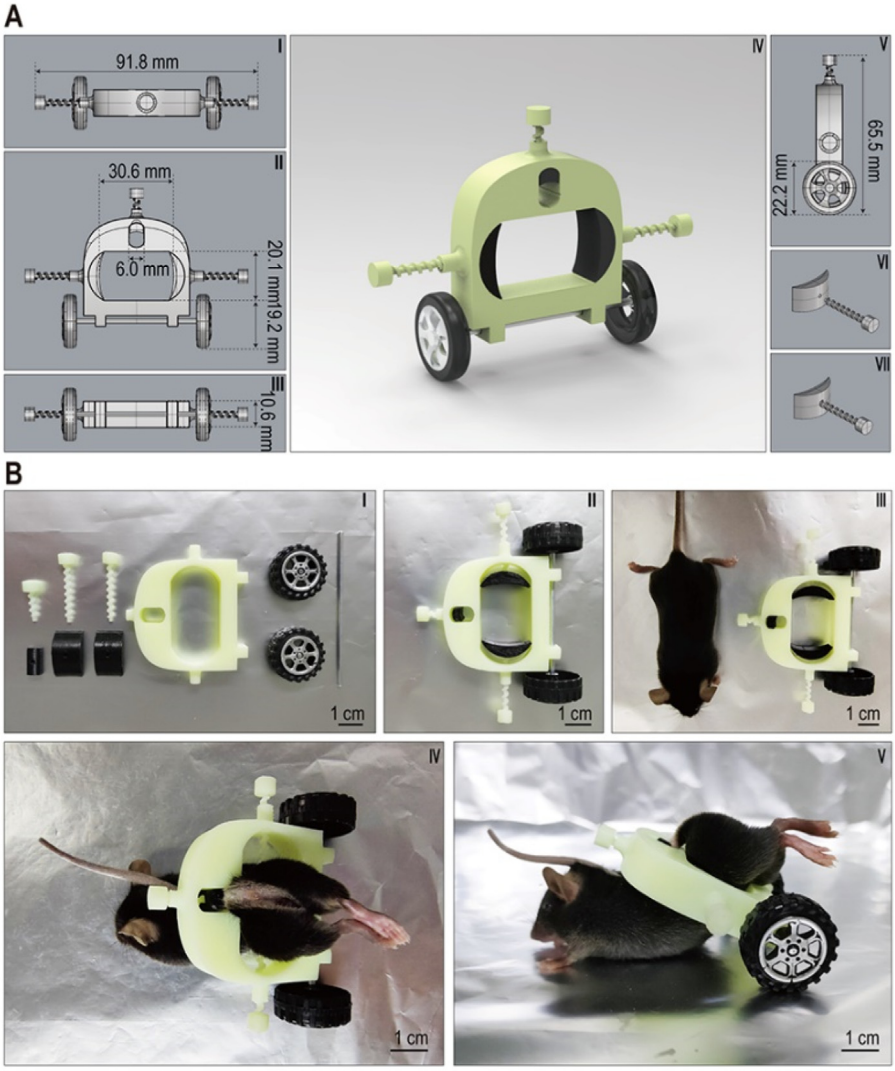

Fig. 1. Establishing a mouse model of disuse osteoporosis using a noninvasive movable 3D-printed unloading device (3D-ULD) (A) Schematic diagram illustrating the design of the 3D-ULD (A–I) top view (A-II) front view (A-III) bottom view (A-IV) stereo view, and (A–V) lateral view of the device and (A-VI and VII) rotary knob and cushion (B) Modelling process of mice unloaded in the 3D-ULD (B–I) separated components of the 3D-ULD (B-II) assembly of the unloading devices (B-III) comparison of a mouse with the 3D-ULD (B-IV and V) top and lateral views of a mouse unloaded in the 3D-ULD. Scale bar: 1.0 cm in all the panels.

body of the mouse and keep the mouse steady in the device. The tail of the mouse was placed in the upper cavity, and the vertical rotary knobs were adjusted to fit the size of its tail. The device was readjusted every three days. Every unloaded mouse was fed in one cage, and sufficient food and water were supplied on the floor of the cage.

2.5. Tail suspension

After anaesthesia, the mice were suspended through their tail according to the recommendations from Morey-Holton and Globus [14]. In brief, steel wire was attached to the top of the cage and allowed to slide easily. Medical tape was used to stick the middle part of the tail of each mouse to the steel wire to suspend the mouse with its hindlimbs in the air and forelimbs on the ground at a head-down angle of approximately 30° (Supplemental Figure 1). Food and water were placed on the ground within reach of the mice. Each mouse was raised in its own cage.

2.6. Micro-CT analysis

Femurs collected from the mice were scanned using micro-CT (micro-CT 50, Scanco Medical, Bassersdorf, Switzerland). The voxel size was set to 14.8 μm (14.8 μm for one scanning layer), and the micro-CT threshold value was set to 212 to 1000. Representative reconstructed images of the cut femur obtained by micro-CT were obtained using the femur growth plate morphology as a reference. For quantitative analysis of the trabecular bone, the region of interest was limited to 100 layers above the distal growth plate of the femur. Representative reconstructed cortical bone images were taken 500 layers above the distal growth plate of the femur. For quantitative analysis of the cortical bone, the region of interest was limited to between 500 and 550 layers above the distal growth of the femur.

2.7. H&E staining

Femurs collected from the mice were decalcified in 10% EDTA solution for 28 days at room temperature, and the decalcification solution was renewed every two days. The bone and vital organs (heart, lung, liver, kidney, spleen and thymus) of the mice were embedded in paraffin and sectioned using a rotary microtome (Thermo Fisher Scientific, Microm HM325, MA, USA) at a thickness of 4 μm. The sections were dewaxed in dimethylbenzene and a graded ethanol series and then stained using an H&E staining kit (BBI, E607318-0206, Shanghai, China) according to the manufacturer's instructions. Images were taken using an inverted microscope (Nikon, DS-Ri1, Tokyo, Japan).

2.8. TRAP staining

The left femur paraffin sections were dewaxed and then stained using

the TRAP Staining Kit (Sigma, 387 A, MO, USA) according to the manufacturer's instructions. Images were taken using an inverted microscope (Nikon, DS-Ri1, Tokyo, Japan). Analyses of the osteoclast number per bone perimeter (Oc.N/B.Pm) and the osteoclast surface per bone surface (Oc.S/BS) on the subepiphyseal region were performed using TRAP staining images according to the standard procedures published by the American Society for Bone Mineral Research [17,18].

2.9. Immunohistochemical (IHC) staining

For IHC staining, an IHC Staining Kit (MXB, KIT-9707, Fujian, China) was used according to the manufacturer's instructions. The femur paraffin slices were incubated with one of the following primary antibodies overnight at 4 °C: anti-DMP1-C (1:200 diluted with PBS) or anti-CTSK (1:300 diluted with PBS). The antibody against DMP1-C (monoclonal, 8G10.3) was a gift from Dr. Chunlin Qin at Texas A&M College of Dentistry. The antibody for CTSK was purchased from Abcam (Santa Cruz, sc-48353, CA, USA). A DAB Kit (MXB, DAB-0037, Fujian, China) was used for visualization. The slices were then counterstained with 2% methyl green solution (Sigma, M8020, MO, USA). Images were taken using an inverted microscope (Nikon, DS-Ri1, Tokyo, Japan). Analyses of the osteoblast number per bone perimeter (Ob.N/B.Pm) and the osteoblast surface per bone surface (Ob.S/BS) on the endosteal surface of midshaft femurs was performed using DMP1-IHC images according to the standard procedures published by the American Society for Bone Mineral Research [17].

2.10. Alkaline phosphatase (ALP) staining

The femur paraffin sections were dewaxed and stained using an ALP Staining Kit (Sangon Biotech, C520019-0005, Shanghai, China) according to the manufacturer's instructions. Briefly, the sections were stained with ALP solution at 37 °C for 30 min and then counterstained with 2% methyl green solution (Sigma, M8020, MO, USA) for 10 min at room temperature.

2.11. Quantitative real-time PCR assay (Q-PCR)

Total RNA tibia was isolated from using the TRIzol reagent (Invitrogen, 15,596–018, MA, USA). The Prime Script RT Reagent Kit with the gDNA Eraser Kit (Takara, RR047A, Kyoto, Japan) was used for cDNA synthesis. Q-PCR was performed with a Light Cycler 96 (Roche, Basel, Switzerland) using a TB Green Premix Ex Taq II Kit (Takara, RR820A, Kyoto, Japan) according to the manufacturer's instructions. The gene expression levels were normalized to the level of the internal housekeeping gene *Gapdh*. The $2^{-\triangle\triangle Ct}$ calculation method was used to calculate the relative mRNA expression levels of the genes. The primer sequences used in this study are listed in Supplemental Table 1.

2.12. Double labelling

Xylenol orange (10 mg/kg, Sigma, 52,097, MO, USA) was intraperitoneally injected into the mice one week before sample collection, and 10 mg/kg calcein (Sigma, C0875, MO, USA) was intraperitoneally injected into the mice 12 h before sample collection. Tibia collected from the mice were embedded in light-cured resin (EXAKT, 7200 VLC, Norderstedt, Germany) for 13.5 h under light exposure. Hard tissue sectioning was performed using a hard tissue sectioning and grinding system (EXAKT, Norderstedt, Germany). The thickness of the sections was set to 20 μm. Analyses of the mineral apposition rate (MAR) and bone formation rate per bone surface (BFR/BS) on the endosteum region were performed using double labelling images according to the standard procedures published by the American Society for Bone Mineral Research [17].

2.13. Von Kossa staining

Femurs collected from the mice were embedded in light-cured resin (EXAKT 7200 VLC, Norderstedt, Germany) for 13.5 h. A hard tissue sectioning and grinding system (EXAKT, Norderstedt, Germany) was used to obtain hard tissue s

ections of the femurs at a thickness of 20 μm. The sections were stained with 2% silver nitrate solution (Sigma, S8157, MO, USA) under strong light for 45 min. After staining with 5% sodium thiosulfate solution (Sigma, 217,263, MO, USA), the sections were counterstained with Nuclear Fast Red solution (BBI, E670101-0100, Shanghai, China) for 15 min at room temperature.

2.14. Three-point bending test

Femurs collected from the mice were subjected to the three-point bending test. The mechanical properties of the femurs were evaluated at mid-diaphysis using an electronic universal testing machine (Suns, UTM2502, Shenzhen, China). Femurs with the physiological curvature facing up were fixed on a supporter with two fixed loading points separated by 3.5-mm gap. A 0.5-mm-thick steel cross bar plate perpendicular to the long axis of the femurs and at the midpoint between two loading points was used to apply a stabilizing preload of 1 N. The bending load was applied at a constant displacement rate of 5 mm/min until fracture occurred, and the internal and external major- and minor-axis lengths of the femur at the fracture point were measured after micro-CT scanning. The maximum load (maximum tensile load that the femur can sustain before failure), ultimate displacement (maximum displacement that the femur can sustain before failure), elastic displacement (maximum displacement that the femur sustains during elastic deformation) and yield load (maximum tensile load that the femur sustains during elastic deformation) were determined from the load–deformation bending curve. The stiffness was calculated according to the formula K=Fp/dp (Fp is the yield load and dp is the elastic displacement). The elastic modulus was calculated according to the formula $E = FpL3/48dpI$ (L is the distance between two supporting points and I is the moment of inertia of the cross-section in relation to the horizontal axis). The moment of inertia of the cross-section in relation to the horizontal axis was calculated according to the formula $I = \pi(BH3\text{-}bh3)/64$ (B is the external major-axis length of the femur at the fracture point, b is the internal major-axis length of the femur at the fracture point, H is the external minor-axis length of the femur at the fracture point, and h is the internal minor-axis length of the femur at the fracture point). The maximum energy absorption was calculated based on the formula U=Fpdp/2, and the bending stress was calculated according to the formula $\sigma = FLH/8I$ (F is the maximum load). The maximum strain was calculated in accordance with the formula $\varepsilon = 12\ dH/2L2$ (d is the ultimate displacement).

2.15. Enzyme-linked immunosorbent assay

Retro-orbital blood was collected before the mice were analysed. In brief, the mice were anaesthetized and placed in a head-down tilt position, and retroorbital blood was then sampled using a blood collection tube, stored at 4 °C overnight, and centrifuged at 3000 rpm for 10 min. The serum supernatant was collected for analysis. The corticosterone serum levels were detected by enzyme-linked immunosorbent assay (ELISA) using a corticosterone enzyme immunoassay kit (KAY, KX-76430, Shanghai, China) according to the manufacturer's instructions. The detection sensitivity was set to 1.0 ng/ml, and the lower limit of detection was set to 1.0 ng/ml.

2.16. Statistics

All the data are presented as the means ± SDs. Significant differences among multiple groups were determined by one-way ANOVA with Dunnett's multiple comparisons test. A P value less than 0.05 was

considered to indicate statistical significance: and these values are labelled as * P < 0.05, **P < 0.01, ***P < 0.001, ****P < 0.0001. GraphPad Prism (version 8.0) was used for the statistical analyses.

3. Results

3.1. A 3D-ULD was generated for the mouse unloading model

To determine the size of the 3D-ULD, we first determined various body parameters of the mice, including the body length, body width, thickness of the tail and position of the hip joint and then used these body parameters as references for designing the 3D-ULD. To appropriately accommodate each mouse, the maximum width and height of the 3D-ULD were set to 91.8 mm and 65.5 mm, respectively (Fig. 1A–I, V). To determine the appropriate angle for each mouse (appropriately 30°) to ensure disuse of their hindlimbs, the height of the bearing surface of the middle cavity was set to 19.2 mm (Fig. 1A–II). Furthermore, to suit the different body sizes of the various mice and their growing bodies, the maximum width and height of the middle cavity were set to 30.6 mm and 20.1 mm, respectively, and the width could be adjusted freely using two rotary cushions (Fig. 1A–II). Fig. 1A–VI and VII show the structure of the rotary cushions. To allow fixation of the tails of the mice, the width of the tail-fixing cavity was set to 6.0 mm, and the space of the cavity could be modulated with an upper rotary cushion (Fig. 1A–II). To achieve a suitable bearing surface area, the thickness of the 3D-ULD was set to 10.6 mm (Fig. 1A–III). A 3D rendering of the 3D-ULD is shown in Fig. 1A–IV. 3D printing technology was used to generate and assemble components of the unloading device (Fig. 1B–I - III). After being anaesthetized, the mice were unloaded easily and steadily in the 3D-ULD (Fig. 1B–IV, V).

3.2. Effective bone loss due to disuse was induced in the mice unloaded in the 3D-ULD

To explore the impact of the 3D-ULD-based unloading method on the disused bones of mice, we collected femurs from mice belonging to the control group, the tail suspension group and the 3D-ULD unloaded group for micro-CT measurements. The mice in the tail suspension group showed a reduced femur length compared with the control mice, whereas the 3D-ULD mice showed a femur length comparable with that of the control mice (Fig. 2B). Obvious trabecular bone loss was observed in the tail suspension and 3D-ULD unloaded groups compared with the control group (Fig. 2A). According to the micro-CT quantitative analysis, the mice suspended by their tail or unloaded in the 3D-ULD displayed significant decreases in bone volume per tissue volume (BV/TV), trabecular number (Tb.N), and trabecular thickness (Tb.Th) (Fig. 2B). Moreover, compared with the tail suspension group, the 3D-ULD group showed more trabecular bone loss and a significant decrease in BV/TV, but no significant differences in Tb.N and Tb.Th were found between these two groups (Fig. 2A and B). In addition, we found significant decreases in the bone mineral density (BMD) in the disused femurs of mice unloaded in the 3D-ULD or suspended by their tail (Fig. 2B). In addition, *von Kossa* staining was performed. As shown in Fig. 2E, lighter *von Kossa* staining and less bone volume were found in the tail suspension and 3D-ULD unloaded groups, and these findings were consistent with the quantitative results from the micro-CT analysis. However, a comparable BMD of disused femurs was found between the mice suspended by their tail and those unloaded in the 3D-ULD (Fig. 2B, E). In addition to trabecular bone parameters, we also analysed cortical bone phenotypes. The micro-CT results showed that both the suspended and unloaded mice exhibited

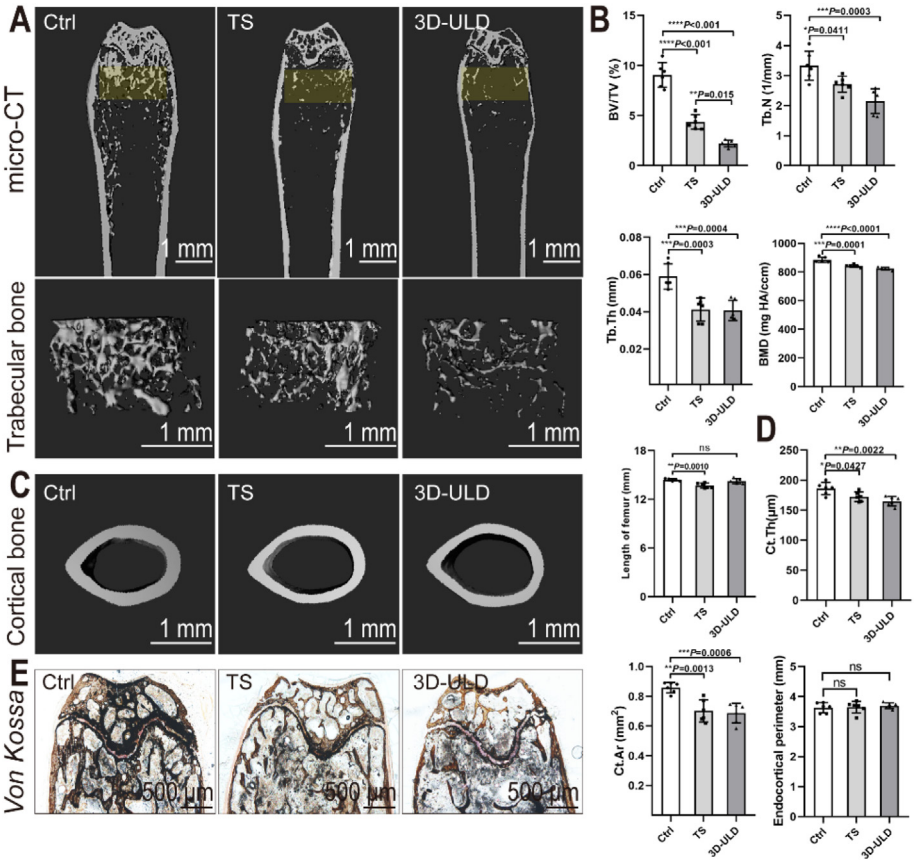

Fig. 2. Bone loss in femurs of mice unloaded in the 3D-ULD (A) Representative micro-CT images showing bone structures and trabecular bone of the femurs of mice belonging to the control, tail suspension and 3D-ULD unloaded groups. Scale bar: 1.0 mm in all the panels. The yellow regions in the upper panels indicate the region of interest for quantitative measurements (B) Micro-CT measurements of bone volume per tissue volume (BV/TV), trabecular number (Tb.N), trabecular thickness (Tb.Th), bone mineral density (BMD) and length in the femurs of mice belonging to the control, tail suspension and 3D-ULD unloaded groups, n = 6 (C) Representative micro-CT images showing the cortical bone of the femurs of mice belonging to the control, tail suspension and 3D-ULD unloaded groups. Scale bar: 1.0 mm (D) Micro-CT measurements of femur cortical bone thickness (Ct.Th), cortical bone area (Ct.Ar) and periosteal perimeter of cortical bone of the mice belonging to the control, tail suspension and 3D-ULD unloaded groups, n = 6 (E) Representative *von Kossa* staining images of femurs of mice belonging to the control, tail suspension and 3D-ULD unloaded groups. Scale bar: 500 μm. The data are presented as the means ± SDs. The significant differences among the three groups were determined by one-way ANOVA with Dunnett's multiple comparisons test. P < 0.05 was considered to indicate statistical significance. *P < 0.05, **P < 0.01, ***P < 0.001, ****P < 0.0001.

thinner cortical bone than the control mice (Fig. 2C). The cortical bone thickness (Ct.Th) and cortical bone area (Ct.Ar) of the femur were significantly lower in the two experimental groups compared with the control group (Fig. 2D). However, no significant difference in cortical bone phenotype was found between the tail suspension group and the 3D-ULD unloaded group (Fig. 2C and D). No differences in the endocortical perimeter of the femur were found among the three groups (Fig. 2D). Moreover, we examined the muscles of the hindlimbs and noted obvious hindlimb muscle atrophy in the mice that were suspended or unloaded (Supplemental Figure 2A). Additionally, we weighed the soleus, gastrocnemius and rectus femoris muscles of the mice and found significant reductions in muscle weight in the two experimental groups (Supplemental Figure 2B). The weights of the hindlimb muscles of the mice unloaded in the 3D-ULD were compared with those of mice in the tail suspension group (Supplemental Figure 2B). To explore the long-term effect of our method on disused bones, we prolonged the unloading time in the 3D-ULD from 1 month to 2 months (Supplemental Figure 3A). According to the micro-CT results, the femurs in mice unloaded in the 3D-ULD for 2 months showed increased trabecular bone loss than those of the mice unloaded for 1 month (Supplemental Fig. 3B and C). Consistently, a thinner cortical bone was found in the mice subjected to an extended unloading time of 2 months (Supplemental Fig. 3B and C).

3.3. Bone resorption was enhanced in mice unloaded in the 3D-ULD

H&E staining results showed that the bone volume of the femurs was markedly decreased in the suspended and unloaded mice (Fig. 3A). Additionally, we explored the alterations in the bone resorption activity of the mice. The TRAP staining results indicated increased osteoclast numbers and enhanced bone resorption activity in the two experimental groups (Fig. 3B). The bone morphometric analysis results similarly indicated that the suspended and unloaded mice showed significantly increased bone resorption parameters, including the osteoclast number per bone perimeter (Oc.N/B.Pm) and the osteoclast surface per bone surface (Oc.S/BS) (Fig. 3D). To further verify the enhancement of bone resorption activity, we conducted anti-CTSK IHC staining. The staining results showed that mice suspended by the tail or unloaded in the 3D-ULD displayed markedly increased CTSK expression in the femurs (Fig. 3C). We also measured the expression levels of bone resorption-related genes, including *Ctsk*, *Trap* and *Mmp9*. Consistently, the Q-PCR results showed that the expression levels of bone resorption-related genes (*Ctsk*, *Trap* and *Mmp9*) in the two experimental groups was significantly higher than those in the control group (Fig. 3E). Taken together, these results suggest that bone resorption was significantly enhanced in the mice unloaded in the 3D-ULD, and similar bone resorption was found with the unloaded and tail suspension groups.

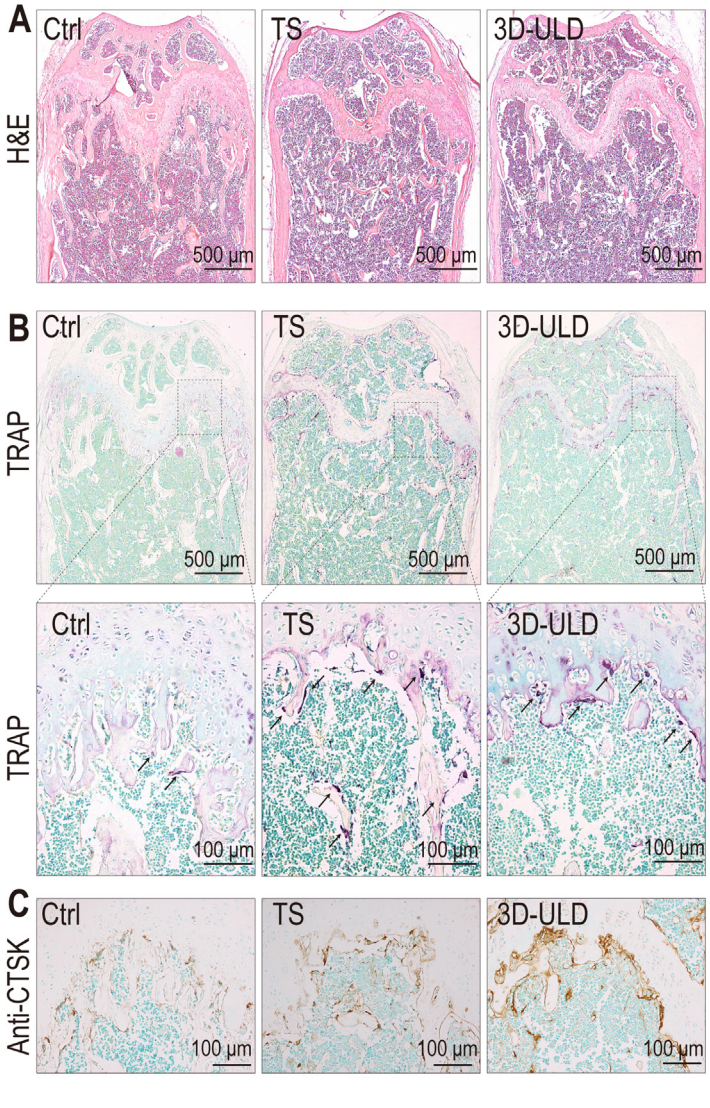

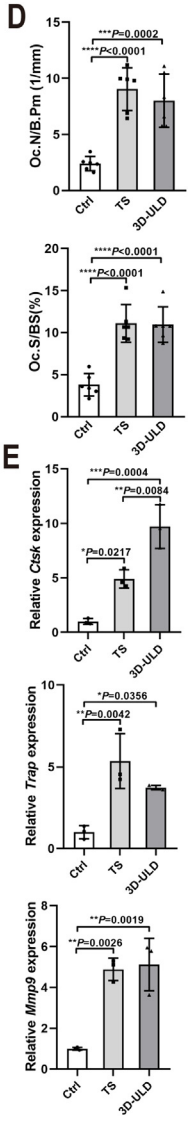

Fig. 3. Enhanced bone resorption in mice unloaded in the 3D-ULD (A) Representative H&E staining images of femurs of mice belonging to the control, tail suspension and 3D-ULD unloaded groups. Scale bar: 500 μm (B) Representative TRAP staining images of femurs of mice belonging to the control, tail suspension and 3D-ULD unloaded groups. Scale bar: 500 μm in the upper panels and 100 μm in the lower panels. The black arrows indicate TRAP-positive osteoclasts (C) Representative anti-CTSK immunohistochemical (IHC) staining images of femurs of mice belonging to the control, tail suspension and 3D-ULD unloaded groups. Scale bar: 100 μm (D) Quantification of osteoclast and bone resorption metrics, osteoclast number per bone perimeter (Oc.N/B.Pm) and osteoclast surface per bone surface (Oc.S/BS) in femurs of mice belonging to the control, tail suspension and 3D-ULD unloaded groups, n = 6 (E) Q-PCR analysis of Ctsk, Trap and Mmp9 expression levels in the tibia of mice belonging to the control, tail suspension and 3D-ULD unloaded groups, n = 3. The data are presented as the means ± SDs. The significant differences among the three groups were determined by one-way ANOVA with Dunnett's multiple comparisons test. $P < 0.05$ was considered to indicate statistical significance. *P < 0.05, **P < 0.01, ***P < 0.001, ****P < 0.0001.

3.4. Osteogenic activity was inhibited in the mice unloaded in the 3D-ULD

The variation in osteogenic activity of the mice was also analysed. To determine the bone formation rate, double labelling was conducted. The mice that were suspended or unloaded exhibited a markedly decreased new bone formation rate (Fig. 4A, C). Bone formation ability was most significantly inhibited in the mice unloaded in the 3D-ULD (Fig. 4A, C). According to the quantitative analysis, the bone dynamic histomorphometric parameters MAR and BFR/BS were markedly reduced in the two experimental groups (Fig. 4B, D). Moreover, the ALP and anti-DMP1 IHC staining results showed that osteogenic activity was substantially inhibited in the disused femurs of mice suspended by the tail or unloaded in the 3D-ULD (Fig. 4E, G). Consistently, the bone morphometric analysis indicated that two bone formation parameters, namely, the osteoblast number per bone perimeter (Ob.N/B.Pm) and the osteoblast surface per bone surface (Ob.S/BS), were significantly decreased in the tail suspension group and 3D-ULD unloaded group (Fig. 4F). Significantly decreased bone formation parameters were found in the 3D-ULD unloaded group compared with the tail suspension group (Fig. 4F). Furthermore, the expression levels of osteogenic genes (*Runx2*, *Alp* and *Dmp1*) were markedly decreased in the two experimental groups (Fig. 4H). Therefore, the tail suspension and the 3D-ULD unloading method significantly inhibited bone formation activity in disused femurs, whereas the inhibition of osteogenic activity induced by the 3D-ULD unloading method was more marked than that induced by tail suspension.

3.5. The mechanical properties of the femurs were attenuated in mice unloaded in the 3D-ULD

We further tested the mechanical properties of femurs using a three-point bending test (Fig. 5A). According to the results, the ultimate force of the disused femurs was significantly decreased in the tail suspension and 3D-ULD unloaded groups (Fig. 5B). Furthermore, the femurs of the suspended and unloaded mice showed obvious decreases in stiffness and the elastic modulus (Fig. 5B). Moreover, the femurs of the two experimental groups exhibited less maximum energy absorption and decreased bending stress than those of the normal control group, as determined by the three-point bending test (Fig. 5B). In addition, the maximum strain on the femurs was significantly increased in the two experimental groups. In summary, the 3D-ULD unloading method effectively attenuated the

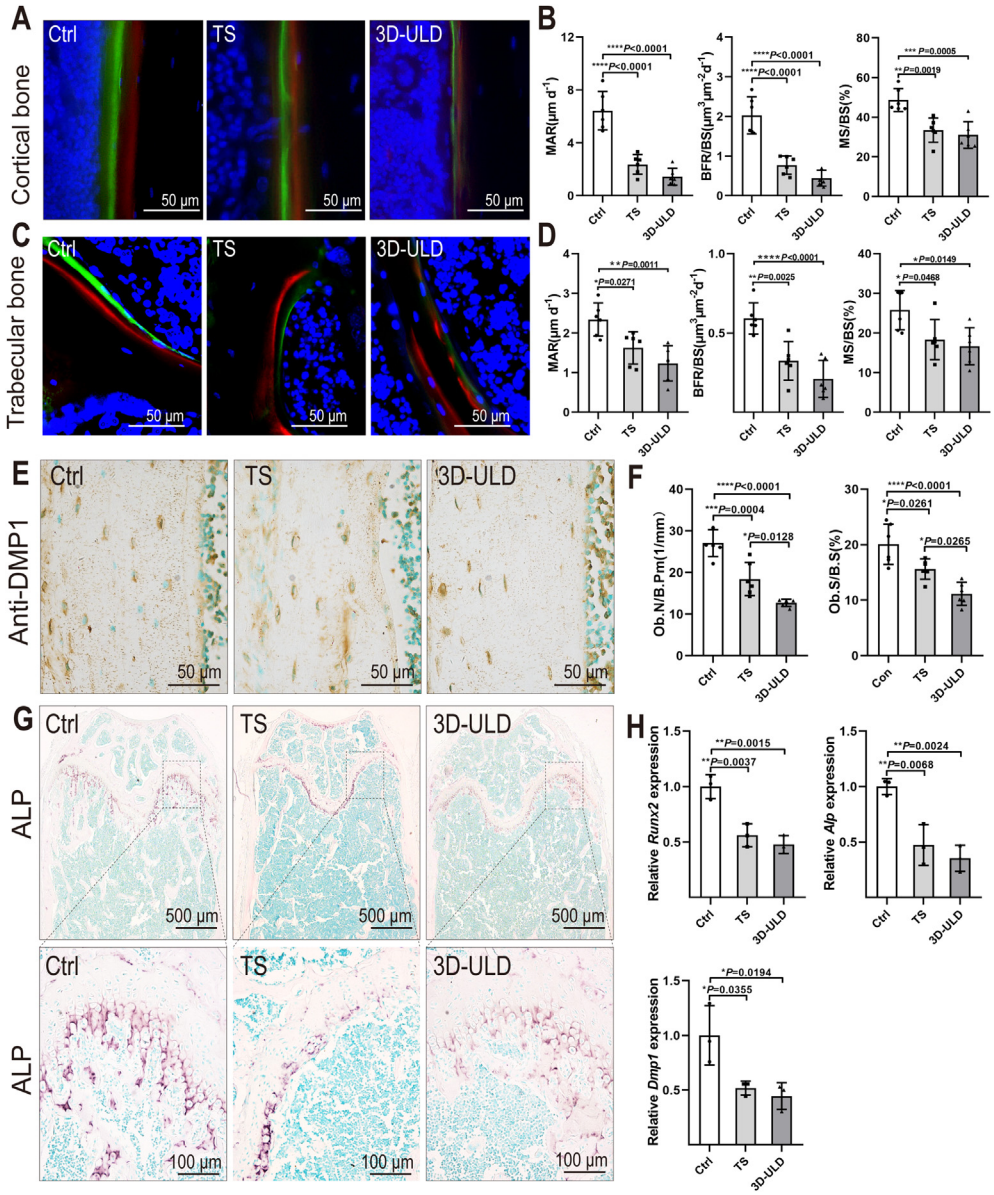

Fig. 4. Inhibition of osteogenic activity in mice unloaded in the 3D-ULD (A) Representative images showing the cortical bone formation rates of the control, tail suspension and 3D-ULD unloaded groups as determined by double labelling with calcein and xylenol orange. Scale bar: 50 μm (B) Bone histomorphometric analysis of the mineralization rate (MAR) and bone formation rate per bone surface (BFR/BS) of cortical bone of the control, tail suspension and 3D-ULD unloaded groups, n = 6 (C) Representative images showing the trabecular bone formation rates of the control, tail suspension and 3D-ULD unloaded groups as determined by double labelling with calcein and xylenol orange. Scale bar: 50 μm (D) Bone histomorphometric analysis of the mineralization rate (MAR) and bone formation rate per bone surface (BFR/BS) of trabecular bone of the control, tail suspension and 3D-ULD unloaded groups, n = 6 (E) Representative anti-DMP1 immunohistochemical staining (IHC) images of femurs of mice from the control, tail suspension and 3D-ULD unloaded groups. Scale bar: 50 μm (F) Quantification of osteoblast and bone formation metrics, osteoblast number per bone perimeter (Ob.N/B.Pm) and osteoblast surface per bone surface (Ob. S/BS) in femurs of mice from the control, tail suspension and 3D-ULD unloaded groups, n = 6 (G) Representative ALP staining images of femurs of mice from the control, tail suspension and 3D-ULD unloaded groups. Scale bar: 500 μm in the upper panels and 100 μm in the lower panels (H) Q-PCR analysis of Runx2, Alp and Dmp1 expression in tibia of mice belonging to the control, tail suspension and 3D-ULD unloaded groups, n = 6. The data are presented as the means ± SDs. The significant differences among the three groups were determined by one-way ANOVA with Dunnett's multiple comparisons test. $P < 0.05$ was considered to indicate statistical significance. *P < 0.05, **P < 0.01, ***P < 0.001, ****P < 0.0001.

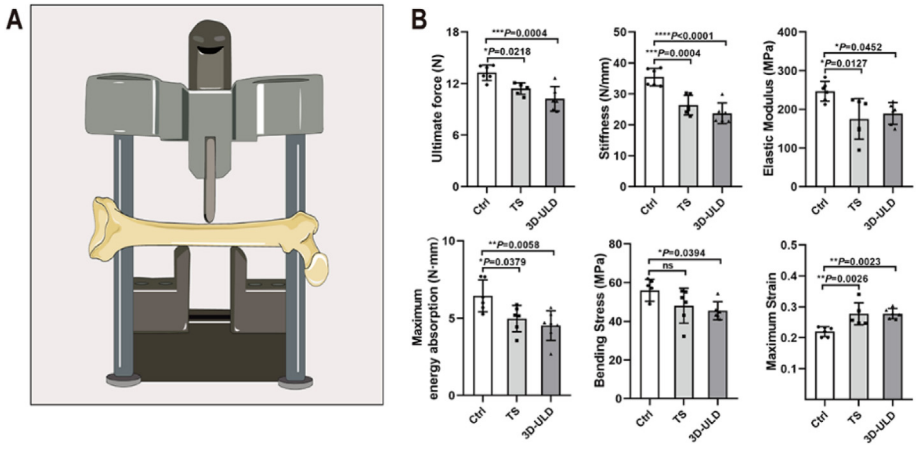

Fig. 5. Attenuated mechanical properties of bone in mice unloaded in the 3D-ULD (A) Schematic diagram illustrating the three-point bending test (B) Analysis of the ultimate force, stiffness, elasticity modulus, maximum energy absorption, bending stress and maximum strain in femurs of mice from the control, tail suspension and 3D-ULD unloaded groups using the three-point bending test, n = 6. The data are presented as the means ± SDs. The significant differences among the three groups were determined by one-way ANOVA with Dunnett's multiple comparisons test. $P < 0.05$ was considered to indicate statistical significance. ns, not significant, *P < 0.05, **P < 0.01, ***P < 0.001, ***P < 0.0001.

mechanical properties of the disused femurs of the mice to levels comparable to those of the mice subjected to the tail suspension method.

3.6. The mice unloaded in the 3D-ULD exhibited alleviated side effects

We subsequently examined the side effects that are usually observed in a mouse suspended by its tail. When a mouse is suspended by its tail, the tail shows evidence of rupture of the skin and a nonphysiological curve (Fig. 6A). However, no obvious tail damage was observed in the mice unloaded in the 3D-ULD (Fig. 6A). Moreover, a significant decline in body weight was detected in mice during the first week of tail suspension (Fig. 6B). The body weight of the tail suspension group was obviously lower than that of the control group. And this decrease may have been induced by chronic mental stress (Fig. 6B). Only a slight decrease in body weight was detected in the mice unloaded in the 3D-ULD (Fig. 6B). Furthermore, the chronic mental stress of the mice was assessed. The

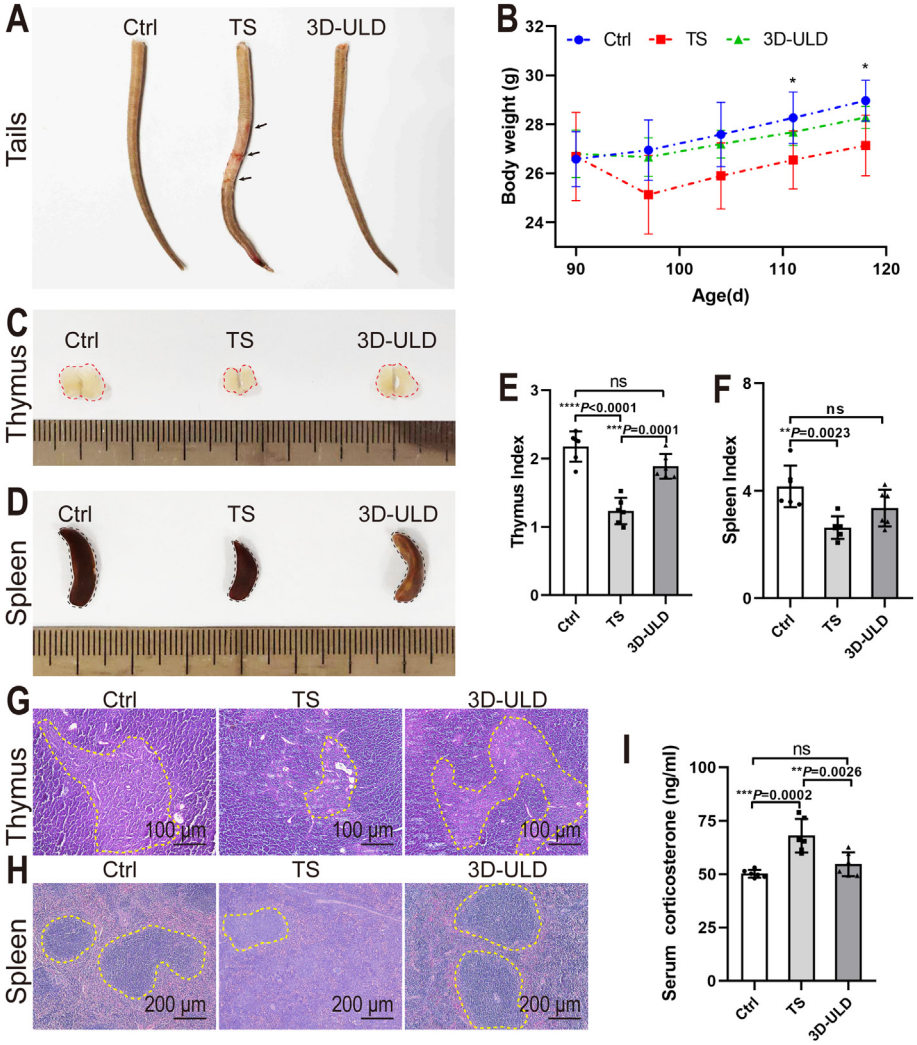

Fig. 6. Alleviated side effects in mice unloaded in the 3D-ULD (A) Images showing tails of the mice belonging to the control, tail suspension and 3D-ULD unloaded groups (B) Analysis of the body weight of mice from the control, tail suspension and 3D-ULD unloaded groups, n = 6. Images showing the thymus (C) and spleen (D) isolated from mice belonging to the control, tail suspension and 3D-ULD unloaded groups. Analyses of the thymus index (E) and spleen index (F) of mice belonging to the control, tail suspension and 3D-ULD unloaded groups, n = 6. Representative H&E staining images of the thymus (G) and spleen (H) of mice from the control, tail suspension and 3D-ULD unloaded groups. Scale bar: 100 μm in (G) and 200 μm in (H) (I) Serum corticosterone levels in mice from the control, tail suspension and 3D-ULD unloaded groups determined by ELISA, n = 6. The data are presented as the means ± SDs. The significant differences among the three groups were determined by one-way ANOVA with Dunnett's multiple comparisons test. $P < 0.05$ was considered to indicate statistical significance. ns, not significant, **P < 0.01, ***P < 0.001, ***P < 0.0001.

mice in the tail suspension group exhibited obvious atrophy of the thymus and spleen (Fig. 6C and D). Consistently, the thymus and spleen indices of the tail suspension group were significantly lower than those of the control group (Fig. 6E and F). Slight atrophy of the thymus and spleen was observed in the mice unloaded in the 3D-ULD, whereas the thymus and spleen indices were not significantly altered in the mice unloaded in the 3D-ULD compared with the control mice (Fig. 6C–F). Moreover, H&E staining showed no marked alteration in the thymus in the unloaded mice, although obvious loss of the medulla of the thymus was detected in the suspended mice (Fig. 6G). In addition, the white pulp of the spleen showed a decrease in area and an unclear demarcation in the tail suspension group, and the demarcation of the white pulp of the spleen was maintained in the 3D-ULD unloaded group (Fig. 6H). Additionally, no obvious differences in the other vital organs (heart, lung, liver and kidneys) were detected among the three groups (Supplemental Figure 4). The serum corticosterone levels were also measured by ELISA, and the results indicated a significant increase in the serum corticosterone levels in the tail suspension group compared with the control group (Fig. 6I). However, the serum corticosterone levels in the 3D-ULD group were significantly lower than those in the tail suspension group. The novelty of this study is summarized in Fig. 7: the mice unloaded in the 3D-ULD exhibited marked decreases in bone mass in the disused hindlimbs but did not suffer from chronic stress, pain or immobilizations.

4. Discussion

Bone loss caused by disuse is more severe than that caused by ordinary primary osteoporosis. Disuse can cause a large amount of bone loss within a relatively short period of time, which results in a high risk of fracture and related diseases [4]. In daily life, the lower limb bone of humans is subjected to three types of mechanical loading, including static gravity-related weight bearing, ground reaction forces and dynamic loading generated by muscle contractions during locomotion. The absence or decrease in mechanical loading results in disuse osteoporosis [19]. For the in-depth study of disuse osteoporosis, it is important to establish a reasonable bionic and stable animal model of disuse osteoporosis. According to previous studies, several types of animal models of disuse osteoporosis have been examined [13]. However, the current models used for investigating disuse osteoporosis face several limitations: (1) Most methods are invasive and harmful to animals. For instance, the tail suspension method may cause sloughing of the tail skin and can even damage the ventral artery and vein of the tail [14,20]. Moreover, circulatory disturbances in the tail make long-term tail suspension impossible [21]. (2) Under the constraints of unloading devices, animals are unable to move freely, which greatly affects the chow intake and mental state of the animals [22,23]. (3) Complicated equipment installation or surgery requires the operators to have certain experience levels, and the unloading effects on animals could show variations among different operators [24,25]. (4) Because the hindlimbs of the animals still show partial weight bearing in some of the established models of disuse osteoporosis, a model with improved consistency is needed [11,26,27]. (5) The growth of an animal and the increases in its body size during the modelling period also need to be considered.

To overcome the abovementioned shortcomings, we designed a noninvasive method for inducing disuse osteoporosis in mice based on 3D printing technology. The approach, which involves support rather than suspension or surgery, does not induce obvious damage to the unloaded mice. Moreover, the movable design allows elevation of the mice at a head-down angle of approximately 30° with their hindlimbs effectively unloaded. The unloaded mice had free access to food and water through the use of their forelimbs. Furthermore, the 3D-ULD, which was designed based on body parameters of the mice, can be freely modulated based on the increasing body size of the growing unloaded mice through rotary knobs. We systematically evaluated this mouse model of disuse osteoporosis in terms of histomorphology, molecular biology, mechanical properties and chronic stress and performed head-to-head comparisons with the model established using the tail suspension method. In previous studies, approximately 45% trabecular bone loss was found in mouse femurs after 1 month of tail suspension [28,29]. According to the results of our study, the mice unloaded in 3D-ULD for 1 month exhibited approximately 70% trabecular bone loss in their femurs, whereas tail suspension for 1 month induced approximately 50% trabecular bone loss, which indicated that bone loss was induced effectively through unloading in the 3D-ULD. This new method resulted in more effective stimulation of trabecular bone loss in unloaded bone. More trabecular bone loss was induced in our unloaded model than in the tail suspension model, and this increased bone loss may have resulted from a reduction in movement and less muscular activation in the hindlimbs of the mice in the 3D-ULD. Moreover, we found that cortical bone gradually became thinner in the mice unloaded using this

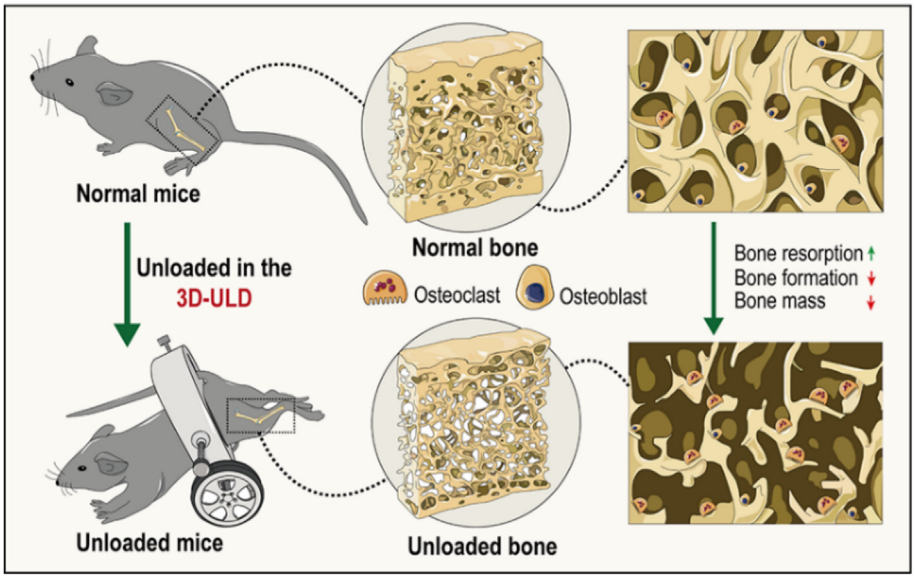

Fig. 7. Schematic representation of bone loss in mice unloaded in the 3D-ULD. Mice unloaded in the 3D-ULD exhibited obvious alterations in the bone structure and bone mass. The unloaded mice exhibited significantly decreased trabecular bone and thinner cortical bone, and these effects mainly resulted from enhanced bone resorption with increased osteoclasts and inhibited bone formation with decreased osteoblasts.

noninvasive method, and 10% cortical bone mass loss in the femur was observed after 1 month of unloading. Previous studies indicated that 1 month of tail suspension results in approximately 10% cortical bone mass loss in mice [28,29], which was consistent with the results observed for the tail suspension group in this study. In terms of stimulating bone loss, our method exerted similar effects as tail suspension.

Bone loss occurs because of an imbalance between bone resorption and bone formation. For example, astronauts lose bone during space flight, exhibiting markedly increased bone resorption [30]. In a long-term 90-day bed rest study in humans, bone loss occurred mainly due to tremendous enhancement of bone resorption [31]. C57BL/6 mice subjected to tail suspension for 2 weeks also exhibited markedly enhanced bone resorption [32]. Moreover, immobilization of mice or rats enhances bone resorption [6,7]. In our mouse model, the bone resorption parameters Oc.N/B.Pm and Oc.S/BS dramatically increased in unloaded 3D-ULD mice. Consistently, the expression levels of bone resorption-related genes, including *Ctsk*, *Trap,* and *Mmp9,* significantly increased. Furthermore, TRAP and anti-CTSK IHC staining showed enhanced bone resorption activity in the unloaded mice. Therefore, the results indicate that enhanced bone resorption plays an important role in the loss of bone observed in the mice unloaded in the 3D-ULD. Notably, human bone formation was found to be inhibited in a long-term bed rest study [31]. We found that bone formation was inhibited in mice after unloading in the 3D-ULD. The poor bone formation observed in the tail suspension group was consistent with the results obtained in previous studies [33,34]. The unloaded mice exhibited a significantly decreased bone formation rate, as determined by double labelling. Moreover, the bone formation parameters MS/BS, MAR, BFR/BS, Ob.N/B.Pm and Ob.S/BS was also significantly reduced in the unloaded mice. Moreover, the expression levels of bone formation-related genes, including *Runx2*, *Alp* and *Dmp1*, were consistently decreased in the mice unloaded in the 3D-ULD. In summary, the observed bone loss was mainly attributed to enhanced bone resorption and inhibited bone formation. In addition to a decreased bone volume, we detected attenuated mineralization in the mouse femurs under unloaded conditions. Additionally, the mice subjected to tail suspension for 1 month exhibited a 10% lower BMD in their femurs [28,29]. Similarly, our results showed that the BMD in the femur was decreased by an average of 10% in the mice unloaded for 1 month, and this loss tendency was maintained with an extended unloading period.

According to previous studies, the bone of patients with osteoporosis exhibits significantly decreased mechanical properties [35,36]. Animal studies have shown that mechanical properties, including maximum load, stiffness, energy absorption, elastic force and elastic modulus, are significantly decreased in mice and rat subjected to tail suspension [37,38]. In this study, we also observed attenuated mechanical properties in the femurs of mice suspended by their tail or unloaded in the 3D-ULD. More importantly, the mechanical test results revealed that the ultimate force, stiffness, elastic modulus, maximum energy absorption and bending stress of the disused femurs of mice unloaded in the 3D-ULD were significantly decreased, and the maximum strain of the disused femurs was markedly increased; these findings were mainly due to bone loss, the thinning of cortical bone, and the attenuation of mineralization.

In our study, we noted an approximately 5% reduction in body weight gain in the unloaded mice compared with the control mice, whereas the mice in the tail suspension group showed a greater reduction in body weight gain; these findings agree with the results from previous studies, which indicated a 10%–18% decrease in body weight gain in mice suspended by their tail for 2 weeks [24,33]. The decrease in the body weight of the mice may have been related to stress suffered during our experiment. Tail suspension could induce chronic stress in mice, which causes an increase in the corticosterone levels and lymphoid organ atrophy [39,40]. In addition to being a common strategy for modelling disuse osteoporosis in animals, tail suspension is also used to stimulate depressive behaviour in mice and to screen for antidepressant drugs [41,42]. Although the mice exhibited a slight decrease in body weight, the mice unloaded in the 3D-ULD did not exhibit obvious loading pain or stress. The corticosterone levels and the lymphoid organ (spleen and thymus) state could reflect the chronic stress state of mice. The mice suspended by their tail suffered from obvious chronic stress, as indicated by increased corticosterone serum levels and decreased spleen and thymus indices. The mice unloaded in the 3D-ULD showed normal corticosterone levels and spleen and thymus indices. Therefore, mice could be unloaded for a long time in the 3D-ULD to stimulate disuse osteoporosis without inducing obvious damage.

The ovariectomized (OVX) and disuse osteoporosis model shows several key differences from the commonly used postmenopausal osteoporosis model. In the OVX model, the main factor resulting in bone loss is a decrease in oestrogen due to ovariectomy [43]. However, a model of disuse osteoporosis is mainly constructed through a reduction in the mechanical stimulation of bone, as can be achieved via tail suspension [44]. According to previous reports, OVX mice with hormone reduction usually exhibit an increased body weight [45]. In contrast, mice showing a disuse phenotype exhibit a decrease in body weight due to a reduction in intake. More than 2 months are needed to establish postmenopausal osteoporosis in mice; however, only 2 weeks to 1 month are needed for the induction of disuse osteoporosis [13]. According to our previous study, an OVX mouse model exhibits approximately 50% trabecular bone loss after 3 months [46]. In a mouse model of disuse osteoporosis, trabecular bone is rapidly lost, and 50% trabecular bone loss is detected after 1 month. Some studies have revealed a decrease in cortical bone thickness in OVX mice, whereas some studies have shown no alteration. The age of the mice subjected to OVX may determine the alteration in cortical bone. In brief, 2-month-old mice undergoing skeletal growth exhibit a decrease in the cortical bone thickness after ovariectomy, and 3-month-old mice with a mature skeleton rarely show alterations in the cortical bone thickness after ovariectomy [47,48]. However, a decrease in cortical bone thickness is detected in mice exposed to disuse conditions for a relatively short period, and this decrease results in attenuated mechanical properties [28]. In a human study, increased cortical porosity was found after long-term immobilization compared with that found with postmenopausal osteoporosis, and this increase was found to be related to lower osteocyte viability and impaired osteocyte connectivity [49],

In this study, the device used for stimulating disuse osteoporosis was printed using 3D printing technology. We believe that the use of 3D-printed models is a simple and accurate method that can be adapted to different types of animal models and different application scenarios. Using the same design ideas and corresponding programs, we speculate that our method could also be applicable for larger animals, such as rats and rabbits.

Moreover, some aspects of our modelling method need to be further optimized. Currently, the device must be monitored to prevent it from causing additional stress to the animals and to prevent it from detaching from the mice. Due to time limitations, the application of 3D-ULD needs to be further characterized in our future work. In addition, more advanced 3D-printing materials could be applied to enhance the portability and stability of this device in the future. Additionally, this study has several limitations. Female mice were not included in the experiment. A previous study showed greater bone loss in both the trabecular and cortical bones of female mice than in male mice after 21 days of unloading [50]. Moreover, the study was initiated with 3-month-old male mice, which are at a stage of slow skeletal growth. Further studies initiated with aged mice with a mature skeleton are needed to make this model applicable for the study of osteoporosis induced by space flight, long-term limb immobilization or bed rest in adults. Based on the results of the present study, the direct connection between muscle atrophy and bone loss remains unclear. Less attention was given to the mechanism underlying disuse osteoporosis, particularly in this new model. Integrin-based focal adhesion and Pizo1 ion channels in osteocytes reportedly play a role in disuse osteoporosis, and this finding may provide a basis for studying the underlying mechanism in our future

studies [51,52]. Moreover, the materials used for printing the unloading device could be updated to make a sufficiently light device, and this topic needs to be addressed in the future.

In summary, this study developed a simple and noninvasive strategy for establishing a stable unloading model. This model could promote disuse osteoporosis-related research and could thus aid the study of bone loss mechanisms in typical unloading situations such as long-term bed rest or space flight. The 3D-ULD can minimize both harm to animals and the impact of unloading on their lives, and the device thus ensures animal welfare. The integration of 3D printing technology and the noninvasive aspect of our experimental approach will provide new ideas and technical support for expanding the application of unloading for the establishment of various animal models.

Authorship contribution statement

Sun Yao: Conceptualization, Writing – review & editing, Supervision, Funding acquisition. Li Junhui: Methodology, Validation, Formal analysis, Investigation, Data curation, Writing – original draft, Writing – review & editing, Visualization, Project administration. Geng Jiangyu: Methodology, Investigation, Writing – review & editing. Lin Tingting: Methodology, Project administration, Writing – review & editing. Cai Mingxiang: Methodology, Project administration, Writing – review & editing. All the authors approved the manuscript submission.

Declaration of competing interest

All the authors declare no conflicts of interest with the contents of this article.

Acknowledgements

This work was supported by grants from the National Science and Technology Major Project of China (2016YFC1102705), the National Natural Science Foundation Projects of China (8206113022, 81822012, and 81771043), the Central Universities Special Foundation Project for Basic Scientific Research of China (kx0200020173386), Shanghai Municipal Science and Technology Major Project (2017SHZDZX01) , the Shanghai Academic Leader of Science and Technology Innovation Action Plan (20XD1424000), and the Shanghai Experimental Animal Research Project of Science and Technology Innovation Action Plan (8191101676).

Appendix A. Supplementary data

Supplementary data to this article can be found online at https://doi.org/10.1016/j.jot.2021.11.009.

References

[1] Sambrook P, Cooper C. Osteoporosis. Lancet (Londn. Engl.) 2006;367(9527):2010–8 [eng].
[2] Hendrickx G, Boudin E, Van Hul W. A look behind the scenes: the risk and pathogenesis of primary osteoporosis. Nat Rev Rheumatol 2015;11(8):462–74 [eng].
[3] Painter SE, Kleerekoper M, Camacho PM. Secondary osteoporosis: a review of the recent evidence. Endocr Pract : Off J Am College Endocrinol Am Assoc Clinic Endocrinol 2006;12(4):436–45 [eng].
[4] Takata S, Yasui N. Disuse osteoporosis. J Med Invest : JMI 2001;48(3–4):147–56 [eng].
[5] Morey ER, Sabelman EE, Turner RT, Baylink DJ. A new rat model simulating some aspects of space flight. Physiol 1979;22(6):S23–4 [eng].
[6] Sakai A, Nakamura T, Tsurukami H, Okazaki R, Nishida S, Tanaka Y, et al. Bone marrow capacity for bone cells and trabecular bone turnover in immobilized tibia after sciatic neurectomy in mice. Bone 1996;18(5):479–86 [eng].
[7] Shaker JL, Fallon MD, Goldfarb S, Farber J, Attie MFWR-. 2721 reduces bone loss after hindlimb tenotomy in rats. J Bone Miner Res 1989;4(6):885–90 [eng].
[8] Rantakokko J, Uusitalo H, Jamsa T, Tuukkanen J, Aro HT, Vuorio E. Expression profiles of mRNAs for osteoblast and osteoclast proteins as indicators of bone loss in mouse immobilization osteopenia model. J Bone Miner Res 1999;14(11):1934–42 [eng].
[9] Lundberg P, Lerner UH. Expression and regulatory role of receptors for vasoactive intestinal peptide in bone cells. Microsc Res Tech 2002;58(2):98–103 [eng].
[10] Weinreb M, Rodan GA, Thompson DD. Osteopenia in the immobilized rat hind limb is associated with increased bone resorption and decreased bone formation. Bone 1989;10(3):187–94 [eng].
[11] Cruess RL, Kan K, Bassett CA. The effect of pulsing electromagnetic fields on bone metabolism in experimental disuse osteoporosis. Clin Orthop Relat Res 1983;173:245–50 [eng].
[12] Morey ER. Spaceflight and bone turnover: correlation with a new rat model of weightlessness. Bioscience 1979;29(3):168–72.
[13] Komori T. Animal models for osteoporosis. Eur J Pharmacol 2015;759:287–94 [eng].
[14] Morey-Holton ER, Globus RK. Hindlimb unloading rodent model: technical aspects. Bethesda, Md : 1985 J Appl Physiol 2002;92(4):1367–77 [eng].
[15] Zhou W, Min G, Xiaoli LI. 3D printing in medicine. J Tissue Eng Reconstruct Surg 2014;4(3). 62-62.
[16] Liaw CY, Guvendiren M. Current and emerging applications of 3D printing in medicine. Biofabrication 2017;9(2):024102 [eng].
[17] Dempster DW, Compston JE, Drezner MK, Glorieux FH, Kanis JA, Malluche H, et al. Standardized nomenclature, symbols, and units for bone histomorphometry: a 2012 update of the report of the ASBMR Histomorphometry Nomenclature Committee. J Bone Miner Res 2013;28(1):2–17 [eng].
[18] Weske S, Vaidya M, Reese A, von Wnuck Lipinski K, Keul P, Bayer JK, et al. Targeting sphingosine-1-phosphate lyase as an anabolic therapy for bone loss. Nat Med 2018;24(5):667–78 [eng].
[19] Lau RY, Guo X. A review on current osteoporosis research: with special focus on disuse bone loss. J Osteoporos 2011;2011:293808 [eng].
[20] Dupont-Versteegden EE, Peterson CA, Bennett P, Fluckey JD, Knox M. Hindlimb unloading in adult rats using an alternative tail harness design. Aviat Space Environ Med 2004;75(8).
[21] Falcai MJ, Louzada MJ, de Paula FJ, Okubo R, Volpon JB. A modified technique of rat tail suspension for longer periods of observation. Aviat Space Environ Med 2012;83(12):1176–80 [eng].
[22] Bederman IR, Lai N, Shuster J, Henderson L, Ewart S, Cabrera ME. Chronic hindlimb suspension unloading markedly decreases turnover rates of skeletal and cardiac muscle proteins and adipose tissue triglycerides. Bethesda, Md : 1985 J Appl Physiol 2015;119(1):16–26 [eng].
[23] Cryan JF, Mombereau C, Vassout A. The tail suspension test as a model for assessing antidepressant activity: review of pharmacological and genetic studies in mice. Neurosci Biobehav Rev 2005;29(4–5):571–625 [eng].
[24] Li J, Yang S, Li X, Liu D, Wang Z, Guo J, et al. Role of endoplasmic reticulum stress in disuse osteoporosis. Bone 2017;97 [eng].
[25] Judex S, Garman R, Squire M, Busa B, Donahue L-R, Rubin C. Genetically linked site-specificity of disuse osteoporosis. J Bone Miner Res : Off J Am Soc Bone Miner Res 2004;19(4):607–13 [eng].
[26] Izawa Y, Makita T, Hino S, Hashimoto Y, Kushida K, Inoue T, et al. Immobilization osteoporosis and active vitamin D: effect of active vitamin D analogs on the development of immobilization osteoporosis in rats. Calcif Tissue Int 1981;33(6):623–30 [eng].
[27] Földes I, Gyarmati J, Rapcsák M, Szöör A, Szilágyi T. Effect of plaster-cast immobilization on the bone. Acta Physiol Hung 1986;67(4):413–8.
[28] Niu YB, Yang YY, Xiao X, Sun Y, Zhou YM, Zhang YH, et al. Quercetin prevents bone loss in hindlimb suspension mice via stanniocalcin 1-mediated inhibition of osteoclastogenesis. Acta Pharmacol Sin 2020;41(11):1476–86 [eng].
[29] Colaianni G, Mongelli T, Cuscito C, Pignataro P, Lippo L, Spiro G, et al. Irisin prevents and restores bone loss and muscle atrophy in hind-limb suspended mice. Sci Rep 2017;7(1):2811 [eng].
[30] LeBlanc AD, Spector ER, Evans HJ, Sibonga JD. Skeletal responses to space flight and the bed rest analog: a review. J Musculoskelet Neuronal Interact 2007;7(1):33–47 [eng].
[31] Watanabe Y, Ohshima H, Mizuno K, Sekiguchi C, Fukunaga M, Kohri K, et al. Intravenous pamidronate prevents femoral bone loss and renal stone formation during 90-day bed rest. J Bone Miner Res 2004;19(11):1771–8 [eng].
[32] Moriishi T, Fukuyama R, Ito M, Miyazaki T, Maeno T, Kawai Y, et al. Osteocyte network; a negative regulatory system for bone mass augmented by the induction of Rankl in osteoblasts and Sost in osteocytes at unloading. PLoS One 2012;7(6):e40143 [eng].
[33] Amblard D, Lafage-Proust MH, Laib A, Thomas T, Ruegsegger P, Alexandre C, et al. Tail suspension induces bone loss in skeletally mature mice in the C57BL/6J strain but not in the C3H/HeJ strain. J Bone Miner Res 2003;18(3):561–9 [eng].
[34] Jing D, Cai J, Wu Y, Shen G, Zhai M, Tong S, et al. Moderate-intensity rotating magnetic fields do not affect bone quality and bone remodeling in hindlimb suspended rats. PLoS One 2014;9(7):e102956.
[35] Ming Ding, Søren Overgaard, 3-D microarchitectural properties and rod- and plate-like trabecular morphometric properties of femur head cancellous bones in patients with rheumatoid arthritis, osteoarthritis, and osteoporosis, J Orthopaedic Trans 28, 159-168, 2021.
[36] He Z, Chu L, Liu X, Han X, Zhang K, Yan M, et al. Differences in subchondral trabecular bone microstructure and finite element analysis-based biomechanical properties between osteoporosis and osteoarthritis. J Orthopaedic Trans 2020;24:39–45 [eng].
[37] Lloyd SA, Bandstra ER, Willey JS, Riffle SE, Tirado-Lee L, Nelson GA, et al. Effect of proton irradiation followed by hindlimb unloading on bone in mature mice: a model of long-duration spaceflight. Bone;51(4):756—764.
[38] Sun Y, Shuang F, Chen DM, Zhou RB. Treatment of hydrogen molecule abates oxidative stress and alleviates bone loss induced by modeled microgravity in rats. Osteoporos Int 2013;24(3):969–78 [eng].

[39] Wang KX, Shi Y, Denhardt DT. Osteopontin regulates hindlimb-unloading-induced lymphoid organ atrophy and weight loss by modulating corticosteroid production. Proc Natl Acad Sci U S A 2007;104(37):14777–82 [eng].
[40] Wei LX, Zhou JN, Roberts AI, Shi YF. Lymphocyte reduction induced by hindlimb unloading: distinct mechanisms in the spleen and thymus. Cell Res 2003;13(6): 465–71 [eng].
[41] Reis-Silva TM, Cohn DW, Sandini TM, Udo MS, Teodorov E, Bernardi MM. Prenatal lipopolysaccharide exposure affects sexual dimorphism in different germlines of mice with a depressive phenotype. Life Sci 2016;149:129–37 [eng].
[42] Reis-Silva TM, Sandini TM, Calefi AS, Orlando BCG, Moreira N, Lima APN, et al. Stress resilience evidenced by grooming behaviour and dopamine levels in male mice selected for high and low immobility using the tail suspension test. Eur J Neurosci 2019;50(6):2942–54 [eng].
[43] Jilka RL, Hangoc G, Girasole G, Passeri G, Williams DC, Abrams JS, et al. Increased osteoclast development after estrogen loss: mediation by interleukin-6. Science 1992;257(5066):88–91 [eng].
[44] DeLong A, Friedman MA, Tucker SM, Krause AR, Kunselman A, Donahue HJ, et al. Protective effects of controlled mechanical loading of bone in C57BL6/J mice subject to disuse. JBMR plus 2020;4(3):e10322 [eng].
[45] Kanaya N, Chen S. Conjugated linoleic acid reduces body weight gain in ovariectomized female C57BL/6J mice. Nutr Res (NY) 2010;30(10):714–21 [eng].
[46] Jin F, Li J, Zhang YB, Liu X, Cai M, Liu M, et al. A functional motif of long noncoding RNA Nron against osteoporosis. Nat Commun 2021;12(1):3319 [eng].
[47] Roberts BC, Giorgi M, Oliviero S, Wang N, Boudiffa M, Dall'Ara E. The longitudinal effects of ovariectomy on the morphometric, densitometric and mechanical properties in the murine tibia: a comparison between two mouse strains. Bone 2019;127:260–70 [eng].
[48] Zhou S, Wang G, Qiao L, Ge Q, Chen D, Xu Z, et al. Age-dependent variations of cancellous bone in response to ovariectomy in C57BL/6J mice. Exp Therapeutic Med 2018;15(4):3623–32 [eng].
[49] Rolvien T, Milovanovic P, Schmidt FN, von Kroge S, Wölfel EM, Krause M, et al. Long-term immobilization in elderly females causes a specific pattern of cortical bone and osteocyte deterioration different from postmenopausal osteoporosis. J Bone Miner Res 2020;35(7):1343–51 [eng].
[50] Squire M, Brazin A, Keng Y, Judex S. Baseline bone morphometry and cellular activity modulate the degree of bone loss in the appendicular skeleton during disuse. Bone 2008;42(2):341–9 [eng].
[51] Rolvien T, Amling M. Disuse osteoporosis: clinical and mechanistic insights. Calcif Tissue Int 2021;(4) [eng].
[52] Hendrickx G, Fischer V, Liedert A, von Kroge S, Haffner-Luntzer M, Brylka L, et al. Piezo1 inactivation in chondrocytes impairs trabecular bone formation. J Bone Miner Res 2021;36(2):369–84 [eng].